J Appl Electrochem (2011) 41:561–576
DOI 10.1007/s10800-011-0262-7

ORIGINAL PAPER

Electrochemical investigation of the roles of oxyanions in chemical–mechanical planarization of tantalum and tantalum nitride

C. M. Sulyma · C. M. Pettit · C. V. V. S. Surisetty · S. V. Babu · D. Roy

Received: 17 May 2010 / Accepted: 13 February 2011 / Published online: 27 February 2011

Abstract Nitrate, sulfate, and phosphate oxyanions are shown to serve as effective surface-modifying agents for low-pressure chemical–mechanical planarization (CMP) of Ta and TaN barrier layers of interconnect structures. The surface reactions that form the basis of this CMP strategy are investigated using cyclic voltammetry, open circuit potential and polarization resistance measurements, and impedance spectroscopy. The results suggest that forming structurally weak layers of surface oxides is crucial to chemically controlling the CMP of Ta/TaN at low polish-pressures. It is shown that in oxyanion-based slurries, this can be accomplished by modifying the sample surfaces with anion-incorporated oxide films of Ta or TaN, which, in turn, can readily be removed with moderate abrasion. Electrochemical results elaborate the reaction mechanisms that lead to anion-modified oxides, such as $Ta_2O_{5(1-x)}(NO_3)_{10x}$, $Ta_2O_{5(1-x)}(SO_4)_{5x}$, and $Ta_2O_{5(1-x)}(PO_4)_{10x/3}$ on both Ta and TaN surfaces in pH-controlled solutions of KNO_3, K_2SO_4, and KH_2PO_4 solutions, respectively.

Keywords CMP · Tantalum · Tantalum nitride · Impedance spectroscopy · Voltammetry

C. M. Sulyma · D. Roy (✉)
Department of Physics, Clarkson University, Potsdam, NY 13699-5820, USA
e-mail: samoy@clarkson.edu

C. M. Pettit
Department of Physics, Emporia State University, Box 4030, Emporia, KS 66801-5087, USA

C. V. V. S. Surisetty · S. V. Babu
Center for Advanced Materials Processing, Clarkson University, Potsdam, NY 13699, USA

1 Introduction

Ta and TaN are used as diffusion barriers in integrated circuits, and chemical–mechanical planarization (CMP) of these barrier layers is an essential component of processing of materials in the fabrication of such circuits [1]. Guided by the International Roadmap for Semiconductors (ITRS) [2], the new strategies for barrier-CMP focus on a reduced down pressure (<2 psi) polishing to prevent structural damages to the underlying "low-k" dielectrics. In addition, since Si-based low-k materials tend to chemically decompose in alkaline media, weakly acidic/neutral slurry solutions often are preferred for CMP [3]. As demonstrated recently by Surisetty et al. [4, 5], it might be possible to meet these new requirements of Ta/TaN CMP in a cost-effective and environmentally compatible approach, by using simple oxyanions like sulfate, nitrate, and phosphate as surface-modifying agents in the polishing slurries. Since these oxyanion solutions do not contain strong complexing agents, post-CMP cleaning of wafers also is relatively straightforward in this approach.

Further development of oxyanion-based slurries can potentially contribute to the advancement of novel CMP technologies in alignment with the ITRS recommendations [2]. However, the mechanisms of surface layer removal by these slurries are not completely resolved as of now. Understanding the CMP mechanism(s) for these specific systems is necessary to explore the full potential of the oxyanion chemistries in this context. This study focuses on this very subject using electrochemical probes of surface reactions. Ta coupons and TaN wafers are employed here as experimental samples with non-alkaline (pH 3–6) abrasive-free slurry solutions of KNO_3, K_2SO_4, and KH_2PO_4. The abrasive-free environment is used to bring out the chemical/electrochemical effects of the surface-modifying oxyanions.

The roles of H_2O_2 (commonly used oxidizer for metal CMP) in controlling the anion-induced effects are tested. Cyclic voltammetry (CV) is employed to examine the faradaic features of Ta and TaN in the test solutions. Certain anodic and cathodic steps operate in coupled modes at the of open circuit potential (OCP), and represent the chemical characteristics of the experimental interface under CMP conditions [6–8]. To probe these effects, OCP transients are examined in light of the CV results. Linear polarization resistances (LPRs) are determined to check if and how the solution-dependent polish rates and the surface activity of Ta are correlated. Fourier transform electrochemical impedance spectroscopy (FT-EIS) is employed to obtain electrode equivalent circuit (EEC) models of the reactive interfaces [9, 10], which clarify further the chemical mechanism of oxyanion-induced CMP of Ta and TaN.

2 Experimental

2.1 Materials

The Ta sample was a 99.95% pure polycrystalline coupon (2.5 cm × 1.8 cm area, 0.1-cm thickness) from Alfa Aesar, with its 1.5 cm × 1.8 cm area per side exposed to experimental solutions. A 2″ diameter TaN wafer (3,000 Å thick, sputtered onto SiO_2 substrate), obtained from Montco Silicon, was cut into rectangular pieces (3.5 cm × 1.0 cm). A fresh piece, with 2.5 cm × 1.0 cm area exposed to the solution was used for each electrochemical experiment. Between subsequent tests, the Ta coupon was polished on a basic polisher (a rotating stainless steel base covered with Buehler Microcloth™) using a paste of 1 μm alumina abrasives and triply distilled water, followed by thorough rinsing with triply distilled water, and drying in a stream of Ar gas. The Ta or TaN sample was employed as the working electrode (WE) in a 125-mL glass cell, along with a Pt-coil counter electrode and a reference electrode of silver chloride. All the voltages quoted in this study refer to the Ag/AgCl scale. A modified copper clip provided electrical connection through the upper (above the solution) part of the WE.

The electrochemical cell was placed in a metal faraday cage on a grounded metal Table. 0.13 M electrolytes of KNO_3, K_2SO_4, and KH_2PO_4 with x wt% H_2O_2 ($x = 0$ or 5) were prepared using triply distilled water and reagent grade chemicals from Aldrich, and were allowed to contain dissolved oxygen from the atmosphere. KOH and HNO_3 were used to adjust the solution pH (3–6). The solution compositions used in these experiments were previously optimized for CMP of Ta [4, 5]. A 3-mm-thick and 1″ diameter Ta disk sample was used for Ta-CMP experiments that employed a Struers® Labopol-5 polisher with a politex x–y groove pad at a down-pressure of 2.0 psi, and the platen speed was maintained at 90 rpm. The polishing slurry containing 0.13 M oxyanion and 5 wt% Nexsil 35A colloidal SiO_2 abrasives (Nyacol) was delivered to the pad at a rate of 50 mL min^{-1}.

2.2 Instrumentation and procedures

The pH values of the solutions were measured before and after each electrochemical treatment to ensure that the test solution remained chemically stable. The electrochemical cell was controlled by a fast potentiostat [11], designed and assembled in the authors' laboratory. LabVIEW™ codes provided experimental commands and data retrieval. OCP transients (for 15 min after introducing the sample to the experimental cell) and CV were collected at the rate of 10 samples per second. The CV scan rate was 10 mV s^{-1}, with upper and lower voltage bounds set at 0.5 V and −0.5 V, respectively. LPR measurements were performed by applying anodic voltage scans at the rate of 10 mV s^{-1} over a range of ±0.05 V around stabilized OCPs.

FT-EIS used a perturbation spectrum of 210 frequencies between 40 kHz and 1.0 Hz, selected according to the criteria of response-sensitive perturbation [11]. The final input A.C. spectrum to the WE was renormalized to maintain the average perturbation amplitude (E_0) for EIS at 2.5 mV. Each impedance spectrum was collected within 10 s, with the D.C. bias set at a stabilized OCP. The rates of typical OCP variations (1.5×10^{-4} mV s^{-1}) under these conditions were at least four orders of magnitude smaller than the rates of the A.C. voltage variations ($\sim E_0 f_{min} = 2.5$ mV s^{-1}) at the lowest frequency ($f_{min} = 1$ Hz) of the A.C. perturbation. This difference was more than sufficient to meet the steady-state requirement of EIS [8, 9], and the data were validated using a frequency-comparison technique [11]. The real (Z') and imaginary (Z'') parts of the impedance spectra were plotted in the Nyquist format, and the plots were subjected to complex nonlinear least square (CNLS) fitting to obtain EEC models using ZSimpWin™. The modulus-weighting scheme was used for CNLS calculations, and only those EECs resulting in ≤5% uncertainties in the calculated impedance elements were accepted.

3 Results and discussion

3.1 Cyclic voltammetry and faradaic characteristics of Ta in H_2O_2-free solutions

Plots (a) in Fig. 1A–C represent current densities (i) as functions of the time (t) elapsed during three consecutive

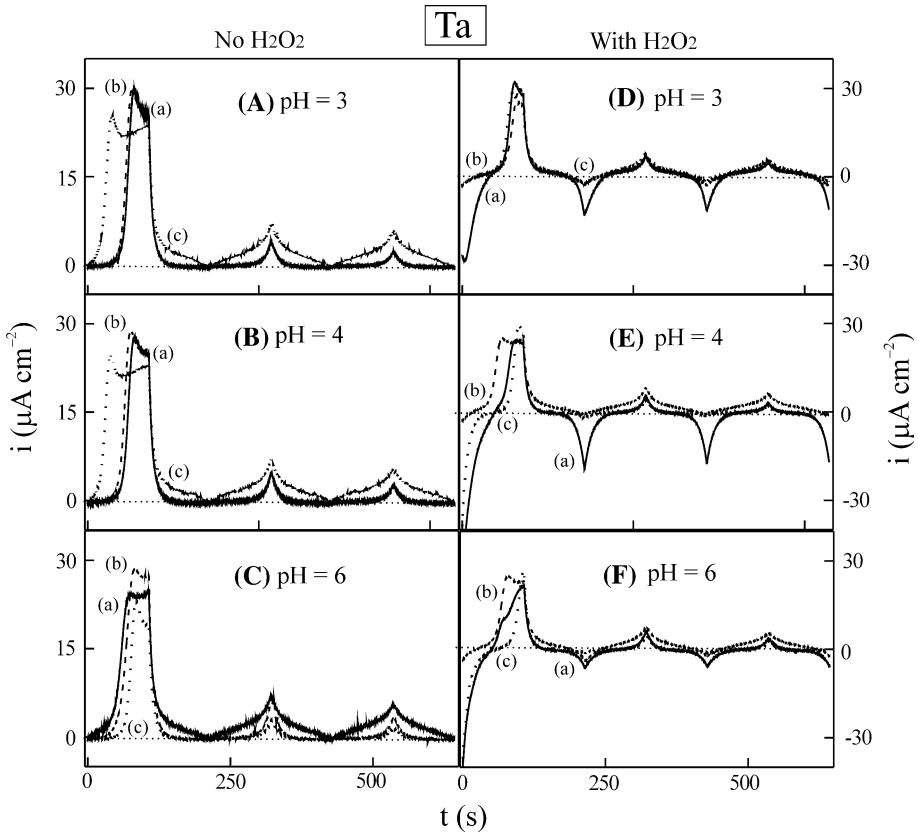

Fig. 1 Unfolded voltammagram for a Ta coupon obtained through three cycles of CV in 0.13 M electrolytes of *a* KNO_3 (*solid line*), *b* K_2SO_4 (*dashed line*) and *c* KH_2PO_4 (*dotted line*) containing 0 (**A**, **B**, and **C**) or 5 (**D**, **E**, and **F**) wt% H_2O_2 at pH 3 (**A** and **D**), 4 (**B** and **E**), and 6 (**C** and **F**). The voltage was scanned at 10 mVs^{-1}

CV cycles of Ta in H_2O_2-free solutions of 0.13 M KNO_3, at pH 3, 4 and 6, respectively. Graphs (b) and (c) in these panels show the corresponding results for 0.13 M K_2SO_4, and KH_2PO_4, respectively. The observed currents are predominantly anodic, indicating the valve metal property of Ta [8]. This current contains a contribution of electro-oxidation without anion incorporation (i_{ox}^{0}), and one affected by anion incorporation (i_{ox}^{in}) [12–15]. Based on the previously published results [12–17], the main steps of these oxidation reactions are schematically shown in Fig. 2, using the sulfate system as an example. The Ta_2O_5 layer shown in Fig. 2 in front of the Ta substrate represents the native oxide of electrochemically untreated Ta, or, a mixture of native and electro-generated Ta_2O_5 of anodically treated Ta. The native oxides are formed by air (and moisture) [10]:

$$4Ta + 5O_2 \rightarrow 2Ta_2O_5. \quad (1)$$

Electro-generation of Ta_2O_5 is a multi-step process [8, 10, 16, 17],

$$5H_2O \rightarrow 10H^+ + 5O^{2-}, \quad (2)$$

$$2Ta \rightarrow 10e^- + 2Ta^{5+}, \quad (3)$$

$$2Ta^{5+} + 5O^{2-} \rightarrow Ta_2O_5, \quad (4)$$

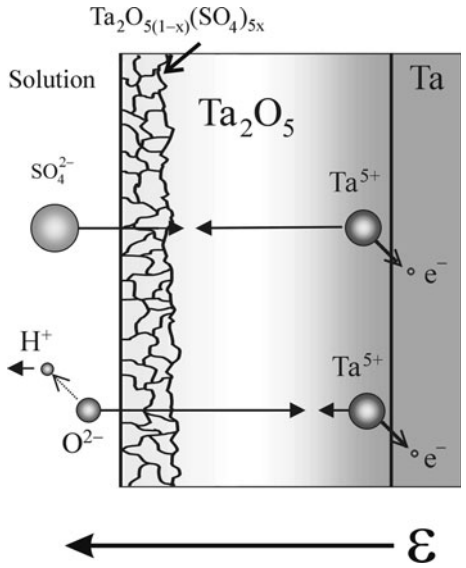

Fig. 2 Schematic diagram (not drawn to scale) indicating the overall process of oxyanion incorporation (shown here for SO_4^{2-}) in anodically formed Ta_2O_5 surface oxides of Ta. The electric field ε within the existing oxide layer supports ion transport within the oxide phase. Driven by this field, Ta^{5+} cations formed at the Ta/oxide interface combine with both the O^{2-} and the SO_4^{2-} anions, leading to the anion-incorporated oxide species $Ta_2O_{5(1-x)}(SO_4)_{5x}$ according to Eq. 7. This anion-modified oxide, formed at the electrode/solution interface, is structurally/chemically different from its underlying anion-free Ta_2O_5

where e^- is the electron charge. Reactions (2) and (3) occur at the oxide–solution and the metal–oxide interfaces, respectively. Reaction (4) occurs through the oxide film, driven by the high electric field ε, which exists within this film due to the anodic overpotential. The net reaction of Eqs. 2–4 is

$$2Ta + 5H_2O \rightarrow Ta_2O_5 + 10H^+ + 10e^-, \quad (5)$$

which generally occurs in the absence of chemisorbing oxyanions in the system [16].

Equation 5 represents the originating reaction of the current i_{ox}^0 [17–19]:

$$i_{ox} = i_A \exp\left[\frac{\beta(E - E_z)}{d}\right], \quad (6)$$

where E and E_z represent the applied voltage and the potential of zero charge (PZC) of the electrode, respectively; d is the average thickness of the Ta_2O_5 film on Ta; i_A and β are constants. In order to support the electric field necessary for reaction (6), the electrode surface requires excess positive charges ($E > E_z$). At the same time, to activate the anodic oxidation current, it is necessary to have $E > E_{oc}$, where E_{oc} is the OCP of the given system. For Ta, $E_{oc} > E_z$ in the most commonly used CMP solutions [12], and hence, in the context of Ta-CMP, the $(E - E_z)$ term in Eq. 6 often is replaced by the applied overpotential, $\eta = (E - E_{oc})$ [8, 10].

As oxyanions from the solution adsorb onto the electrode, they compete with the O^{2-} anions to react with the Ta^{5+} cations generated within the oxide film via reaction (3). Thus, in the presence of oxyanions, reaction (4) occurs in parallel with a simultaneous reaction taking place between the oxyanion and Ta^{5+} [13, 14]. For instance, in K_2SO_4 at pH 3–6, the SO_4^{2-} anions are adsorbed (possibly accompanied by a minority number of co-adsorbed HSO_4^-) [20] at the solution–oxide interface. Being driven by ε, the SO_4^{2-} anions migrate within the oxide layer (Fig. 2), and subsequently, join O^{2-} ions to react with the Ta^{5+} cations migrating from the opposite direction [13]:

$$2Ta^{5+} + 5(1-x)O^{2-} + (5x)SO_4^{2-} \rightarrow Ta_2O_{5(1-x)}(SO_4)_{5x}, \quad (7)$$

where $x < 0.5$ in the most cases [13]. The net reaction of Eqs. 2, 3, and 7, which forms the sulfate-incorporated oxide layer, can be written as

$$2Ta + mH_2O + (5x)SO_4^{2-} \rightarrow Ta_2O_m(SO_4)_{5x} + 10e^- + 2mH^+, \quad (8)$$

where $m = 5(1 - x)$ and $Ta_2O_{5(1-x)}(SO_4)_{5x}$ represents the anion-incorporated Ta-oxide formed at the solution side of the existing oxide layer.

Oxyanion reactions similar to that of Eq. 7 also occur for NO_3^- and $H_2PO_4^-$ [13, 15]:

$$2Ta^{5+} + 5(1-x)O^{2-} + (10x)NO_3^- \rightarrow Ta_2O_{5(1-x)}(NO_3)_{10x}, \quad (9)$$

$$2Ta^{5+} + 5(1-x)O^{2-} + (10x/3)PO_4^{3-} \rightarrow Ta_2O_{5(1-x)}(PO_4)10_{x/3}, \quad (10)$$

where, for Eq. 10, the adsorption of $H_2PO_4^-$ (predominant anion from $K_2H_2PO_4$ at pH 3–6) on Ta_2O_5 is assumed to be dissociative [21, 22]. Addition of Eqs. 2 and 3 with Eq. 9 or 10 will give the net step of anion-incorporated oxidation with nitrate or phosphate, respectively.

Anodic formation of the aforementioned ion-doped oxide species on Ta has been characterized previously by non-electrochemical techniques including transmission electron microscopy and secondary ion mass spectroscopy [13]. Results of these earlier studies have shown $x = 0.27$–0.30 for typical ion contents of various oxyanion-incorporated films of tantalum pentoxide. These chemically modified oxide films have substantially lower dielectric functions in comparison with anion-free Ta_2O_5 [13], and hence, are expected to have reduced mass density and structural integrity. This structural attribute of the anion-modified Ta-oxide is schematically indicated in Fig. 2 by the "brittle" form of the oxide layer in contact with the solution. It is this decreased mechanical strength of the anion-incorporated oxides, which plays a crucial role in surface layer removal in low-pressure CMP of Ta using oxyanion-based polishing slurries.

Cracks and pinholes within the anion-modified oxide layers of Ta tend to alter the usual cathodic response of this valve metal [13, 15]. Owing to this reason, a small cathodic component of i (~ 1 μA cm^{-2}, not clearly visible on the current scale of Fig. 1A–C) was detected in CV. This cathodic current comes from the reduction of O_2 dissolved in the solution, with charge transfer taking place through small openings in the Ta_2O_5 film [23, 24]:

$$O_2 + 4H^+ + 4e^- \rightarrow 2H_2O. \quad (11)$$

The predominant (anodic) part of the current observed in Fig. 1 is i_{ox} [16, 17], with both its i_{ox}^0 and i_{ox}^{in} components having the same voltage dependence according to Eq. 6. As the first anodic scan is applied to a freshly polished Ta surface, a quasi-steady state is achieved when the mutually competing increments of E and d in Eq. 6 become comparable [8]. This effect is observed after the first sharp rise of the currents measured for each system in Fig. 1A–C. Small-amplitude current oscillations, arising from metastable corrosion sites [25, 26] also are observed in these data.

After the first CV cycle is completed, anodically grown Ta_2O_5 passivates the Ta surface [16–18], as is indicated by the drastically lowered values of i in the subsequent CV cycles. This effect of surface passivation can be quantified according to the formula [16–18],

$$\Delta d = \frac{V_{ox}}{zF}\int_0^{t_0} i\mathrm{d}t, \tag{12}$$

where Δd is the incremental growth of the anodic Ta_2O_5 surface film introduced by a given CV cycle; z is the number of electrons involved in the oxidation step; $z = 10$ in the absence of anion incorporation, and $10x$ or $10x/3$ for anion incorporation according to Eqs. 7 (and 9), or 10, respectively; V_{ox} is the molecular volume (50.6 cm^3 mol^{-1}) of Ta_2O_5 [17]; and F and t_0 are the Faraday constant, and the time necessary to complete a CV cycle, respectively. The maximum values of Δd (for $z = 10$ with $x = 0$ in Eqs. 7, 9 and 10) supported by CV cycles 1, 2, and 3 are denoted here as Δd_1, Δd_2, and Δd_3, respectively. These parameters, obtained by applying Eq. 12 to the data (for $i \geq 0$) in Fig. 1A–C are listed in Table 1. A comparison of Δd_1, Δd_2, and Δd_3 indicates how the Ta electrode surface is irreversibly passivated after the first CV scan, with little additional oxides grown in the subsequent cycles.

3.2 Cyclic voltammetry and faradaic characteristics of Ta in H_2O_2-containing solutions

The CV experiments considered in Fig. 1A–C were repeated using the same oxyanion solutions that also contained 5 wt% H_2O_2. The results are shown in the right column of Fig. 1 with plots (a), (b), and (c) representing KNO_3, K_2SO_4, and KH_2PO_4 solutions, respectively. The native Ta_2O_5 layer of Ta in this case is not only formed by reaction (1), but also by H_2O_2 [8, 10]:

$$2Ta + 2O_2 + H_2O_2 \rightarrow Ta_2O_5 + H_2O. \tag{13}$$

Owing to this additional oxidation, the initial Ta surface in Fig. 1D–F is more passivated (allowing lower anodic currents) than the corresponding cases in Fig. 1A–C. The faradaic oxidation steps, as well as the overall voltage dependence of i_{ox} in Fig. 1D–F can still be described by Eqs. 5 and 6, respectively. The predominant cathodic step in H_2O_2-containing acidic solutions is [8, 23]:

$$H_2O_2 + 2H^+ + 2e^- \rightarrow 2H_2O, \tag{14}$$

where the presence of H^+ as a primary reactant restricts the reaction from occurring above the maximum solution pH (6) used here. In addition to this reaction, Eq. 11 could also have a minor contribution to the cathodic currents detected.

Oxyanions on partially oxide-coated metals can adsorb on both oxide-free and oxidized sites of the surface [5, 26, 27], and can enhance co-adsorption of H_3O^+ [28] at these sites. This co-adsorption of hydrated protons seems to be operative here with PO_4^{3-} and SO_4^{2-} on Ta/Ta_2O_5, which limits the adsorption of H_2O_2 on the Ta electrode in KH_2PO_4 and K_2SO_4. This in turn keeps the cathodic currents of reaction (14) relatively small for plots (b) and (c) in Fig. 1D–F. In the nitrate solution at pH 3–4, NO_3^- appears to be comparatively less effective in blocking the adsorption of H_2O_2 on Ta/Ta_2O_5. Such an effect would explain why the cathodic currents of H_2O_2 reduction indicated by plots (a) are larger than those of plots (b) and (c) in Fig. 1D and E. At pH 6, as the concentration of H^+ necessary to support reaction (14) drops, the associated cathodic currents also become small for all the three solutions considered in Fig. 1F. The values of

Table 1 Effective thicknesses of anodically grown oxide layers on Ta and TaN in oxyanion solutions

S. no.	Solution[a]	Δd_1 (nm)[b]	Δd_2 (nm)[b]	Δd_3 (nm)[b]
1	KNO_3, pH 3	718, 391	43.8, 384	21.0, 382
2	KNO_3, pH 4	618, 474	49.2, 473	26.6, 467
3	KNO_3, pH 6	839, 296	227, 288	203, 286
4	K_2SO_4, pH 3	695, 368	41.8, 350	22.3, 348
5	K_2SO_4, pH 4	728, 406	56.6, 395	30.7, 392
6	K_2SO_4, pH 6	719, 462	74.5, 384	37.8, 374
7	KH_2PO_4, pH 3	1115, 489	233, 487	213, 485
8	KH_2PO_4, pH 4	1093, 455	233, 433	212, 431
9	KH_2PO_4, pH 6	440, 424	29.6, 388	14.5, 379
10	$KNO_3 + H_2O_2$, pH 3	596, 432	173, 486	151, 848
11	$KNO_3 + H_2O_2$, pH 4	444, 538	54.5, 536	29.2, 540
12	$KNO_3 + H_2O_2$, pH 6	437, 484	67.1, 484	40.2, 483
13	$K_2SO_4 + H_2O2$, pH 3	533, 367	182, 373	153, 376
14	$K_2SO_4 + H_2O_2$, pH 4	831, 544	236, 546	211, 522
15	$K_2SO_4 + H_2O_2$, pH 6	711, 564	212, 562	182, 565
16	$KH_2PO_4 + H_2O2$, pH 3	643, 529	239, 538	215, 538
17	$KH_2PO_4 + H_2O_2$, pH 4	370, 389	43.2, 401	21.4, 409
18	$KH_2PO_4 + H_2O_2$, pH 6	272, 460	49.9, 459	26.4, 456

[a] All solutions are of 0.13 M salt concentration

[b] The first and the second numbers in each row represent results for Ta and TaN electrodes, respectively

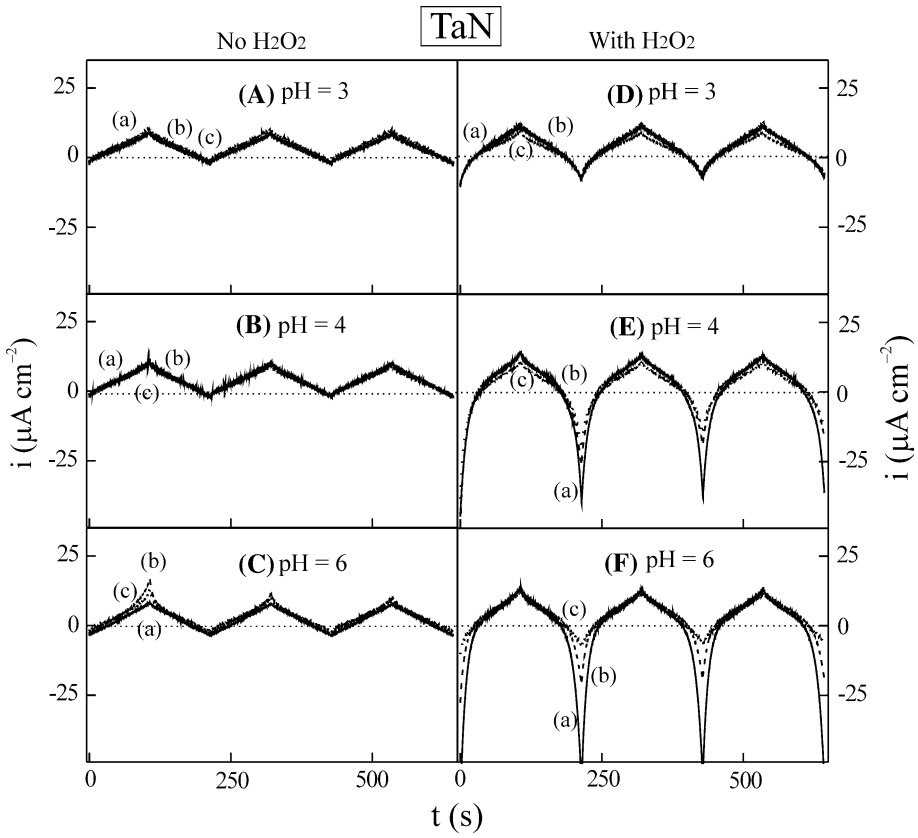

Fig. 3 Unfolded voltammagram for a TaN wafer obtained through three cycles of CV in 0.13 M electrolytes of *a* KNO_3 (*solid line*), *b* K_2SO_4 (*dashed line*) and *c* KH_2PO_4 (*dotted line*) containing 0 (**A**, **B**, and **C**) or 5 (**D**, **E**, and **F**) wt% H_2O_2 at pH 3 (**A** and **D**), 4 (**B** and **E**), and 6 (**C** and **F**). The voltage was scanned at 10 mVs^{-1}

Δd_1, Δd_2, and Δd_3, calculated by combining the CV data of Fig. 1D–F with Eq. 12 are listed in Table 1; these results are similar to those obtained for the corresponding H_2O_2-free systems of Fig. 1A–C.

3.3 Cyclic voltammetry and faradaic characteristics of TaN in H_2O_2-free solutions

Unfolded voltammograms for TaN, recorded in 0.13 M solutions of (a) KNO_3, (b) K_2SO_4, and (c) KH_2PO_4 at three different pH settings are shown in Fig. 3A–C. The noise-like features of these currents are due to current oscillations mentioned in the context of Fig. 1, and have been discussed elsewhere [12, 26]. The voltammetric behavior of TaN is governed by both its native surface oxides and its oxide-free sites. Although the general formula "TaN" is commonly used to describe tantalum nitride wafers in the context of CMP, these wafers typically contain Ta-deficient TaN as well as Ta-rich (Ta_2N or $TaN_{y\leq 0.5}$) sites [29–35], and the latter are particularly susceptible to forming native Ta_2O_5 [36–38]: $4TaN_{y\leq 0.5} + (5/2)O_2 \rightarrow 2TaN_{2y} + Ta_2O_5$; $2(Ta_2N) + (5/2)O_2 \rightarrow 2TaN + Ta_2O_5$. Because the TaN wafers used in this study were deposited on a SiO_2 substrate, the substrate interface could also form native oxides as: $2Ta + SiO_2 + [(3 + n)/2]O_2 + (y/2)N_2 \rightarrow Ta_2O_5 + SiO_nN_y$ [39]. Under anodic voltage activation and in the absence of anion-induced effects, surface oxides on TaN can grow as follows [40]:

$$Ta_2N + 5H_2O \rightarrow Ta_2O_5 + 10H^+ + 10e^- + (1/2)N_2, \quad (15)$$

$$2TaN_{y\leq 0.5} + 5H_2O \rightarrow Ta_2O_5 + 10H^+ + 10e^- + 2N_{y\leq 0.5} \quad (16)$$

The nitrogen species generated via Eqs. 15 or 16 dissolves in the bulk sample and leads to stoichiometric conversion of non-stoichiometric Ta-rich sites [39]:

$$Ta_{2+y}N + (y/2)N \rightarrow [1 + (y/2)]Ta_2N. \quad (17)$$

Direct anodic oxidation of Ta-deficient TaN is likely to cause N_2 evolution: $2TaN + 5H_2O \rightarrow Ta_2O_5 + 10H^+ + 10e^- + N_2$. However, since no bubbles were observed on the TaN electrode surface during CV using H_2O_2-free solutions, such a reaction most probably was not strongly favored. Thus, the anodic currents observed in Fig. 3 originate mostly from reactions (15) and (16). In addition, anodic generation of some tantalum oxynitride (TaON) is possible [40]: $TaN + H_2O \leftrightarrow TaON + 2H^+ + 2e^-$. The relatively small cathodic currents in Fig. 3A–C are associated with reaction (11) [8].

Oxyanions are expected to affect anodic oxidation of TaN. For example, if sulfate ions are present in the solution, the anion-modified version of Eq. 15 could have the form [12]:

$$Ta_2N + mH_2O + 5x(SO_4^{2-}) \rightarrow Ta_2O_{5(1-x)}(SO_4)_{5x} + 2mH^+ + 10e^- + (1/2)N_2, \quad (18)$$

with $m = 5(1 - x)$. Similar reactions of tantalum nitride in nitrate and phosphate solutions would give rise to $Ta_2O_5(1 - x)(NO_3)_{10x}$ and $Ta_2O_5(1 - x)(PO_4)_{10x/3}$, respectively [26].

The faradaic oxidation currents of tantalum nitride, both with and without anion incorporation, can be empirically expressed using Eqs. 6 and 12. In this description, the discontinuities (due to the presence of the N-sites) in the Ta-oxide film can be accounted for in a phenomenological approach by writing: $d \approx d_0\theta$ [41]. Here, d_0 is the average thickness of the oxide-coated regions, and θ is the lateral surface coverage of Ta_2O_5 on TaN. According to Güntherschulze and Betz's description of Eq. 6 [18], $\beta = (zal|e|)/(k_BT)$ in Eq. 6, where k_B and T, represent the Boltzmann constant and the ambient temperature, respectively; and a is the activation distance of O^{2-}, which, for a symmetric potential barrier, is half the jump-distance of O^{2-} during the transport of this ion in Ta_2O_5 [19]. If θ is relatively small, that is $\beta \ll (d/|E - E_z|)$, then the exponential term of Eq. 6 will be linear in E. Because E is scanned as a linear function of t in CV, the resulting expression of i_{ox} under this condition becomes linear in t, and the voltammetry data in Fig. 3A–C represent such a case. This suggests that the density of surface sites containing Ta_2O_5 on TaN is small compared to that of Ta in the corresponding solutions.

The values of Δd_1, Δd_2, and Δd_3, determined by applying Eq. 12 to Fig. 3 are listed in Table 1. In the first CV cycles, Δd_1 for TaN is considerably smaller than the corresponding Δd_1 for Ta. Furthermore, the values of Δd for TaN change only by relatively small amounts during successive CV cycles, whereas those in the case of Ta drop significantly after the first oxidation cycles. These are expected observations, because surface passivation of TaN due to anodic oxide formation only occurs on a limited fraction of surface sites (yielding small values of θ) that are Ta-rich according to Eqs. 15, 16, and 18. In addition, anion-incorporated oxidation could be more effective for TaN than for Ta. The oxide layers formed on TaN under such conditions should be more porous than those formed on Ta under similar experimental conditions, and hence, should continue to allow further anodic reactions in successive CV cycles, as seen in Fig. 3.

3.4 Cyclic voltammetry and faradaic characteristics of TaN in H_2O_2-containing solutions

Voltammetry data for the TaN-H_2O_2 systems are presented in Fig. 3D–F, where the presence of some current oscillations [12] can also be noted. The initial oxide of tantalum nitride in these experiments may contain Ta_2O_5 and TaON formed by H_2O_2 [40]:

$$Ta_2N + H_2O_2 + 2O_2 \rightarrow Ta_2O_5 + H_2O + (1/2)N_2, \quad (19)$$

$$TaN + H_2O_2 \rightarrow TaON + H_2O, \quad (20)$$

with the nitrogen resulting from reaction (19) being consumed by reaction (17). The cathodic currents in Fig. 3D–F are quite noticeable, and their pH dependencies are different from those of the corresponding currents observed for Ta in Fig. 1D–F. It is likely that catalytic electroreduction of H_2O_2 on TaN occurs via a different route than that supported by Ta, and involves the following step [42]: $H_2O_2 + 2e^- \rightarrow 2OH^-$. The OH^- product of this reaction would become more stable with increasing solution pH, and the relatively higher cathodic currents observed at the higher pH settings in Fig. 3D–F are consistent with this mechanism. The anion specificity of TaN is similar to that for Ta discussed in the context of Fig. 1D–F.

3.5 Correlation of electrochemical and CMP results

Polish rate (PR) data for CMP of Ta using H_2O_2 containing slurries of nitrate, sulfate, and phosphate solutions have recently been reported [4]. These CMP results are compared in Fig. 4a with electrochemical LPR data obtained for the corresponding solutions. The LPRs, denoted here as R_p, were determined in the neighborhood of the individual system-OCPs by using the Stern-Geary formalism [8, 24]: $R_p = \mathrm{Lim}_{\eta\rightarrow 0}\,(\partial i/\partial\eta)^{-1}$. Since double layer contribution to the measured current is relatively small [8, 10], one may assume that $i = i_{ox}^0 + i_{ox}^{in}$ in the anodic voltage region near the OCP. According to the above definition of R_p, this implies that [42]

$$R_p = [(R_{ox}^0)^{-1} + (R_{ox}^{in})^{-1}]^{-1}, \quad (21)$$

where R_{ox}^0 and R_{ox}^{in} are the equilibrium charge transfer resistances for the formation of Ta-pentoxide with and without anion incorporation, respectively; $(R_{ox}^0)^{-1} = (\partial i_{ox}^0/\partial\eta)$ and $(R_{ox}^{in})^{-1} = (\partial i_{ox}^{in}/\partial\eta)$. The LPR provides a direct measure of the surface reactivity of the test sample, with smaller values of R_p representing higher chemical activity.

In Fig. 4a, the boxed numbers represent the correspondingly numbered solutions listed in Table 1, and the linear fit to the data yields a coefficient of determination (R^2) at 0.84. Although the PRs were obtained with mechanical polishing of Ta, these data in Fig. 4a display a

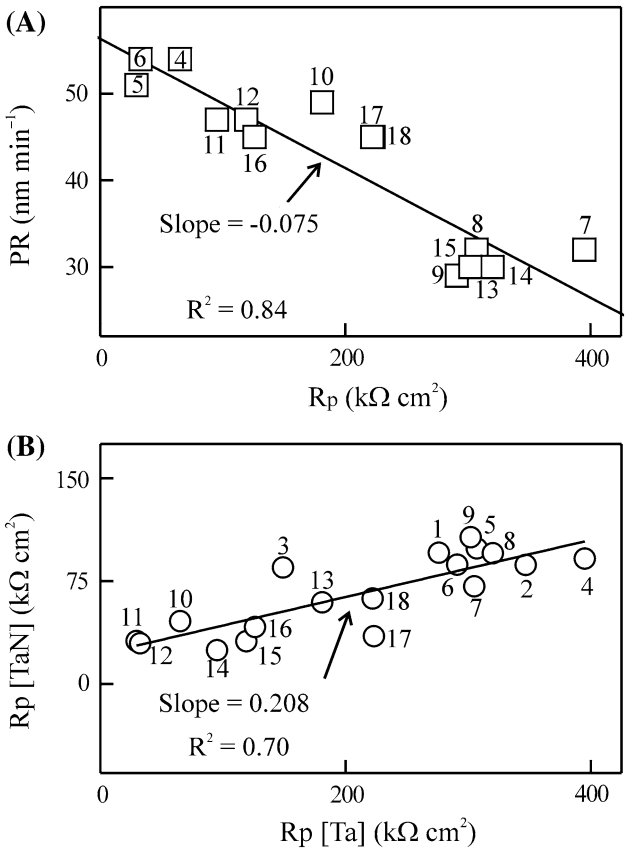

Fig. 4 **a** Ta polish rates (PRs) measured in CMP experiments using different oxyanion-based slurry solutions, correlated with electrochemically measured polarization resistances (R_p) of a Ta coupon electrode in the corresponding solutions. **b** Comparison of the polarization resistances of a TaN wafer electrode (R_p [TaN]) and a Ta coupon electrode (R_p [Ta]), measured in different oxyanion-based solutions. In both **a** and **b**, the numbers used for labeling the individual data points represent the correspondingly numbered solutions listed in Table 1

measurable correlation with R_p recorded in the absence of mechanical abrasion of the sample. The higher PRs corresponding to the decreasing LPRs represent a signature feature of chemically promoted CMP [8], and the anion-incorporation mechanism discussed in the context of Figs. 1, 2, 3 falls in this latter category.

During CMP, the anion-affected, structurally weak Ta-oxide layers are chemically formed on Ta, and removed by low-pressure mechanical abrasion of the polishing pad. As oxide-free areas of the Ta surface are exposed in this process, further oxides, coupled with anion incorporation, are formed due to chemical reactions of Ta with the solutions. This repeated growth and removal of the oxide layers lead to the PRs plotted in Fig. 4a. The latter data follow the inverse solution-dependent trend of the correspondingly measured LPRs, as the variations of both the PR and the LPR share the same chemical origin, namely, the anion-modified oxides.

Figure 4b compares LPR results for TaN obtained from these experiments with the corresponding findings for Ta. The numbered data points represent correspondingly numbered solutions in the list of Table 1. The linear fit to these data indicates an assessable correlation ($R^2 = 0.70$) between the LPR values of Ta and TaN. Based on this observation, it is expected that CMP of TaN using the oxyanion solutions should have PR trends similar to those found for Ta in Fig. 4a.

In the CMP of Ta, entire surface layers might be removed in the form of anion-incorporated Ta-pentoxide, whereas for TaN, these oxide sites would form on a relatively smaller Ta-rich fraction of the sample surface. However, the structural integrity of the full surface region of tantalum nitride would still be lowered by the distributed oxide species, and mechanical abrasion of CMP under this condition would remove both the oxidized and un-oxidized sites of TaN [40]. H_2O_2 increases the overall thickness of the tantalum oxide surface layer, which, in the presence of anions, eventually serves as the primary source of mechanically removable material during CMP). Thus, the LPRs for TaN are in general smaller than those found for Ta using the corresponding solutions. This is consistent with Fig. 3, where the TaN surface shows negligible passivation in comparison with Ta.

3.6 Considerations for surface oxidation and anion incorporation under open circuit conditions of CMP

Oxidation reactions, such as those proposed in Eqs. 5, 8, 15, 16, and 18 as the underlying mechanisms of chemically enhanced CMP of Ta and TaN in oxyanion-based solutions, involve charge transfer across the electrode–solution interface. On the other hand, the CMP results of Fig. 4a were obtained at OCPs in the absence of any external voltages available to activate these charge transfer steps. The PR–LPR correlation, observed in Fig. 4a implies that the oxidation reactions of Ta and TaN can remain active under OCP conditions. As noted in Ref. [8], this is possible due to the mixed potential corrosion mechanism [7], where electrons generated by anodic reactions are consumed by simultaneously active cathodic reactions that have higher Nernst potentials than their anodic counterparts. For instance, the standard potentials (E^0) of reactions (5) and (11) are −0.95 and 0.2 V (vs. Ag/AgCl), respectively [23]. According to the mixed-potential theory, these two reactions can occur in a coupled mode, leading to the net reaction (1), which does not require a net charge transfer across the interface. Similarly, reaction (14) ($E^0 = 1.92$ V vs. Ag/AgCl) could also support reaction (5) [23]. Under these circumstances, the effective OCP (mixed potential) of the combined system would settle between the equilibrium

potentials of the mutually coupled anodic and cathodic steps involved.

In the description of Fig. 2, the surface oxidation and anion-incorporation reactions require a strong interfacial electric field pointing toward the solution side. If the sample surface contains excess positive charges at E_{oc} (that is, $E_{oc} - E_z > 0$), then this field is readily established at $E = E_{oc}$, since the oxide layer thickness under CMP conditions is small (Table 1). For partially oxidized metal surfaces, these charges (q) have two components, q_{ox} and q_m, associated with the oxide-covered and oxide-free parts of the surface, respectively. The value of q_{ox} is determined by the difference between the solution pH and the isoelectric point (IEP) of the oxide sites [8]: $q_{ox} = F$ ([M–OH_2^+]–[M–O^-]), where [M–O]$^-$ and [M–OH_2]$^+$ are the surface concentrations of negatively and positively charged hydroxylated oxide sites of the metal (M), respectively. The value of q_m is dictated by the relative values of E_z and E_{oc} [8, 10]. The calculated PZC for Ta is −1.06 V [12], which generally falls well below the OCPs of Ta measured in commonly used CMP solutions (this is also demonstrated later in the context of Fig. 5). This leads to relatively large positive values of the term ($E_{oc} - E_z$), and since $q_m \propto (E_{oc} - E_z)$ [14], the q_m component of Ta can readily provide excess positive surface charges at E_{oc}.

If the surface of Ta (TaN) is largely covered by native oxides, then q_{ox}, determined by the IEP of the oxide, plays a more critical role than that of q_m in determining the net electrode charges. The commonly cited IEP of Ta_2O_5, measured in oxyanion-free solutions, is 2.8 [43], but in the presence of oxyanions, this IEP tends to shift to much higher values [12]. The amount of this shift depends on the type and concentration of the anion used [44], as for example, an IEP of 5.2 has been measured for Ta_2O_5 in 2 mM $NaClO_4$ [45]. The mechanisms responsible for such anion-induced positive shifts of IEPs may include adsorption of counter-ions at the M-O^- sites, and co-adsorption of protons with anions [12]. H_2O_2 in the solution can also indirectly contribute to upward shifting of IEPs, because Ta_2O_5 films formed in the presence of H_2O_2 have many openings [46], and H^+ from the solution enters these openings to form M-OH_2^+ sites within the pores of the oxide film [47]. Owing to these effects, even in the absence of external voltages, the Ta and TaN electrode surfaces can retain excess positive charges in the pH range explored here. These surface charges support the electric field necessary to oxidize these samples at E_{oc} [48]. OCP transient measurements, discussed in the next section, were performed to verify this concept.

3.7 Open circuit potential variations of Ta and TaN

Figure 5 shows the OCP variations of Ta, measured for 15 min after introducing the sample in different

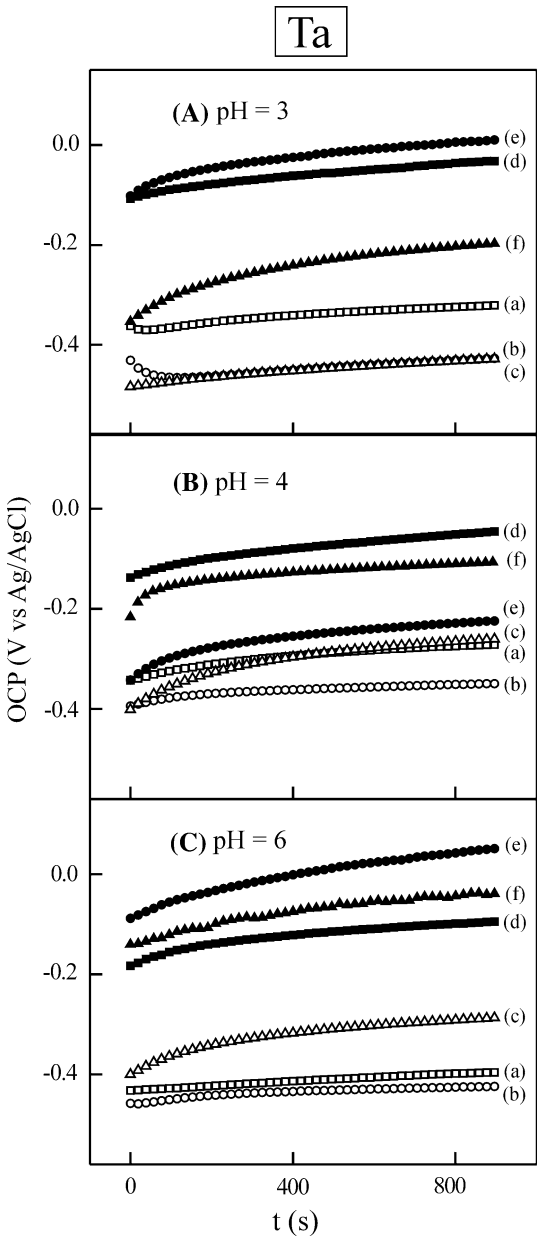

Fig. 5 Open circuit potentials for a Ta coupon electrode, measured as functions of time (t) after introducing the electrode in the experimental cell containing different oxyanion-based solutions. The plots with open (*a–c*) and closed (*d–f*) symbols represent solutions of 0 and 5 wt% H_2O_2 contents, respectively. The *squares* (plots *a* and *d*), *circles* (*b* and *e*), and *triangles* (*c* and *f*) represent nitrate, sulfate, and phosphate solutions (all 0.13 M), respectively

electrolytes. According to mixed potential theory [7, 8], oxide formation on Ta should increase E_{oc}, while anion incorporation in these oxides should reverse this trend; the observed OCP transients would be the net result of these mutually competing effects. For all the cases considered in Fig. 5, E_{oc} increases with increasing time, suggesting that the oxidation reactions (5) and (8) (and similar ones for nitrate and phosphate) dominate the observed OCP

behavior of Ta. These data demonstrate how oxidation of Ta occurs under the OCP conditions of CMP. The values of E_{oc} for the H_2O_2 added solutions (closed symbols) are relatively higher, due to the additional Ta_2O_5 formed in these cases according to Eq. 13. The comparative positions of E_{oc} for the different anions in Fig. 5 are determined by the relative rates of oxide formation and anion incorporation within the oxide layer for the individual systems.

The OCPs continue to increase as the oxide film thickness d increases. However, the electric field ε that supports this oxide growth is inversely proportional to d [19]. Therefore, if the oxide film is not removed by abrasion or dissolution, the strength of ε gradually drops with the oxide growth and eventually the oxidation reactions slow down and stop when E_{oc} is eventually stabilized. When present in the solution, H_2O_2 breaks down during the experiment ($2H_2O_2 \rightarrow 2H_2O + O_2$), and as a result, OCP stabilization of these systems generally takes longer times. This can be seen in some of the closed symbol plots in Fig. 5.

Figure 6 shows OCP transients for TaN, measured employing the same solutions and procedures used for Fig. 5. In the H_2O_2-added solutions (solid symbols), the OCP behaviors of TaN are very similar to those of Ta, indicating predominenance of the growth mode of surface oxides. Reactions 15–17 and 18 (as well as similar ones for nitrate and phosphate) contribute to these oxide growths indicated by these data. The E_{oc} plots for the H_2O_2-added systems appear above those of the H_2O_2-free systems (open symbols in Fig. 6), indicating the presence of relatively higher amounts of surface oxides in the former case. For all the H_2O_2-free solutions in Fig. 6, the E_{oc} plots exibit an initial drop, and often continue to drop for a considerable interval. This occurs due to anion incorporation in the initially present native oxides of TaN.

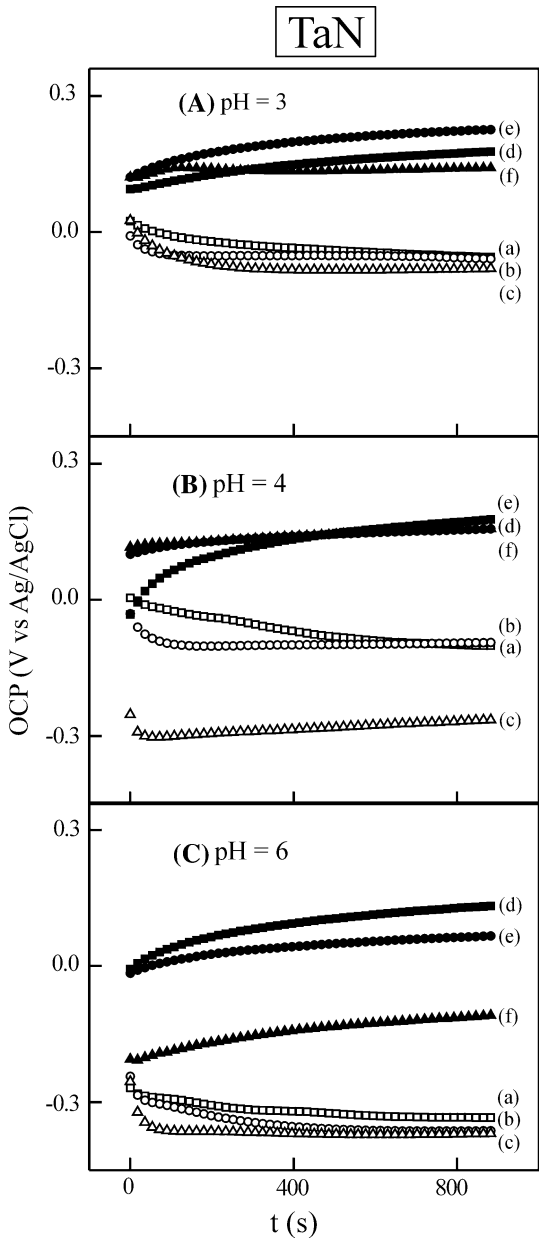

Fig. 6 Open circuit potentials for a TaN wafer electrode, measured as functions of time (t) after introducing the electrode in the experimental cell containing different oxyanion-based solutions. The plots with open (a–c) and closed (d–f) symbols represent solutions of 0 and 5 wt% H_2O_2 contents, respectively. The *squares* (plots a and d), *circles* (b and e), and *triangles* (c and f) represent nitrate, sulfate, and phosphate solutions (all 0.13 M), respectively

3.8 Adsorption characteristics of oxyanions on Ta and TaN determined using FT-EIS

A.C. FT-EIS was employed to study the oxyanion adsorption kinetics and the associated double layer effects. Nyquist spectra for Ta are shown in Fig. 7, where the insets present detailed features of the high-frequency spectra. The symbols and the lines represent experimental data and CNLS calculated fits to the data, respectively. Figure 8a, which represents a standard model of anion adsorption on oxidized metals [27, 41], shows the CNLS-analyzed EEC obtained for Ta. R_u is the uncompensated solution resistance, which essentially remains around 0.5 Ω cm^2. The capacitive reactance of the electrochemical double layer is affected by the intrinsic inhomogenity of the overall surface, and appears in the form of a frequency dispersed constant phase element (CPE). Q_{dl} is an effective CPE that contains a series combination of the double layer and oxide layer CPEs of Ta. The complex impedance $Z(Q_{dl})$ of this effective CPE is defined as [9, 49]: $Z(Q_{dl}) = [Y_{0dl}(j\omega)^n]^{-1}$, where Y_{0dl} is the frequency independent part of the double layer admittance; $j = \sqrt{-1}$; ω is the angular frequency of the A.C. perturbation, and $0 \leq n \leq 1$.

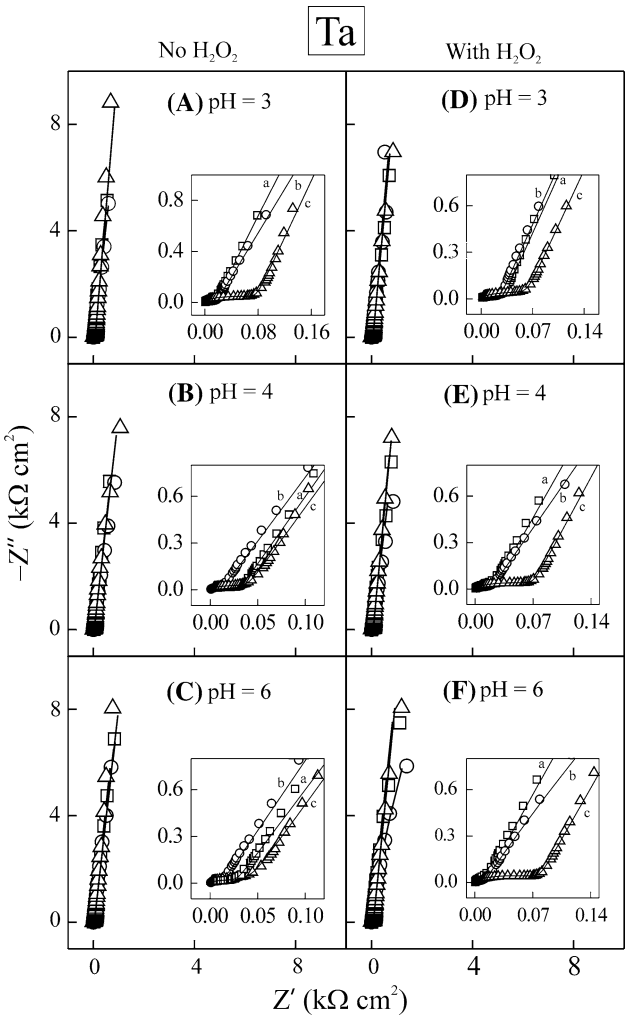

Fig. 7 Nyquist spectra for a Ta coupon electrode recorded at stabilized OCPs in different oxyanion solutions containing 0 (**a**–**c**) or 5 (**d**–**f**) wt% H_2O_2 at pH 3 (**a** and **d**), 4 (**b** and **e**) and 6 (**c** and **f**). The symbols denote experimental data points, with the *squares*, *circles*, and *triangles* representing 0.13 M solutions of KNO_3, K_2SO_4, and KH_2PO_4, respectively. The *lines* are CNLS fits to the data using the circuit model of Fig. 8a. The insets show close-ups of the high frequency spectra on optimized scales

R_{ad} and Q_{ad} are the resistive and the frequency-dispersed CPE components of the adsorption impedance, respectively. The adsorption CPE indicates that the surface inhomogenity of Ta, which is manifested in the double layer characteristics, is also detected in the distribution of the anion adsorption sites. Both branches of the EEC in Fig. 8a are D.C. blocking. The faradaic currents i_{ox}^{0} and i_{ox}^{in}, discussed in the context of D.C. CV, flow through R_p defined in Eq. 21. In the description of Fig. 8a, R_p would be placed in parallel with the R_{ad}–C_{ad} branch. Nevertheless, consistent with previous EIS studies of similar systems [8, 10], and as explained previously in detail [8, 12, 26, 50], R_p is not detected here because of the A.C. shunts provided by the $\{Q_{dl}(R_{ad}–C_{ad})\}$ combination.

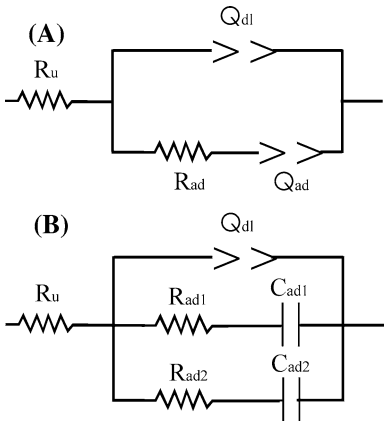

Fig. 8 EEC models used to CNLS-fit the experimentally obtained Nyquist shown in **a** Fig. 7 and **b** Fig. 9. The EEC in **a** for Ta and the one in **b** for TaN apply to all the electrolytes listed in Table 1

Figure 9 presents the Nyquist plots recorded for TaN, with the insets showing close-ups of the high-frequency spectra. The symbols denote experimental data and the lines represent CNLS fits to the data using the EEC of Fig. 8b. This EEC for TaN contains two adsorption branches (R_{ad1}–C_{ad1}) and (R_{ad2}–C_{ad2}), which can be associated with two types of surface sites of TaN, namely the Ta-rich and Ta-deficient sites discussed in the context of the CV results. The net admittance of the $\{Q_{dl}(R_{ad1}–C_{ad1})(R_{ad2}–C_{ad2})\}$ combination was found to be much larger than the polarization conductance ($1/R_p$)[12], and hence, like the case of Ta, R_p has not been included in Fig. 8b. Similarly, the values of R_u for TaN essentially came out to be the same as those found for Ta. Because both the adsorption branches in Fig. 8b contain pure capacitive elements rather than CPEs, the chemical identity of each type of adsorption site does not vary significantly across the electrode surface. This spatial homogeneity of site distribution can be interpreted as the Ta-rich active (oxide-forming) sites having a single chemical makeup, such as Ta_2N (but not a widespread mixture of Ta_2N and $TaN_{y\leq 0.5}$), throughout the surface.

The CPE parameters Y_{dl} and n provide an overall description of how the time constants for double layer charge/discharge are distributed. The interdependencies of these two quantities are checked in Fig. 10a and b for the Ta and TaN, respectively. The boxed numbers represent correspondingly the numbered solutions listed in Table 1. For both electrodes, these data show a continuous drop in the value of n following the correspondingly increasing Y_{dl0}. Larger values of Y_{dl0} imply that more sites per unit area participate in the double layer charge/discharge process. For a microscopically non-uniform surface, this corresponds to the inclusion of more in-homogeneity (and possibly more surface roughness) in the overall EIS response of the electrochemical double layer. A decrease in

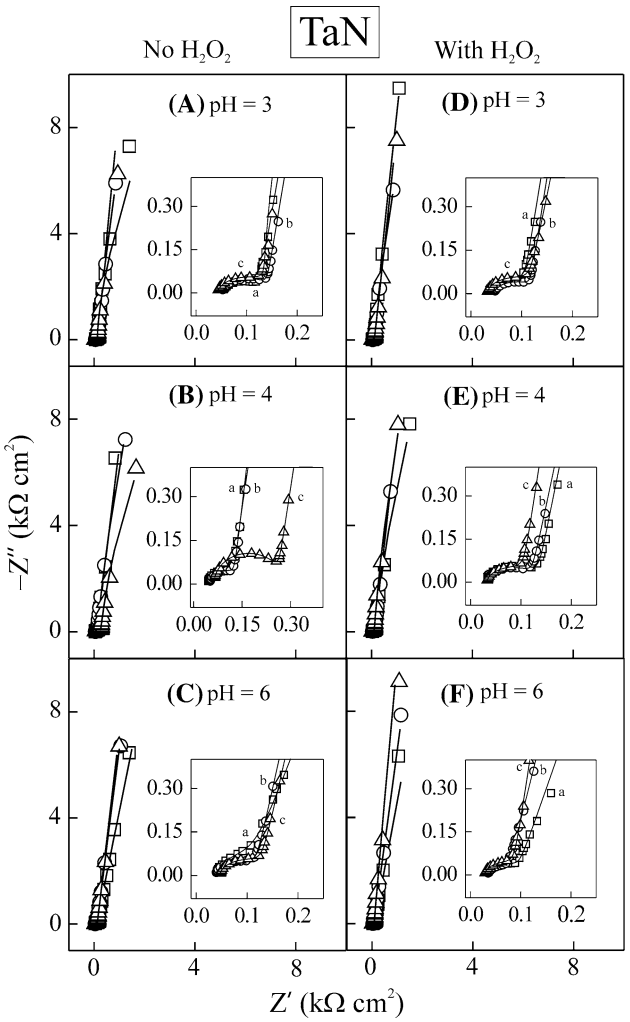

Fig. 9 Nyquist spectra for a TaN wafer electrode recorded at stabilized OCPs in different oxyanion solutions containing 0 (**a**–**c**) or 5 (**d**–**f**) wt% H_2O_2 at pH 3 (**a** and **d**), 4 (**b** and **e**), and 6 (**c** and **f**). The symbols denote experimental data points, with the *squares*, *circles*, and *triangles* representing 0.13 M solutions of KNO_3, K_2SO_4, and KH_2PO_4, respectively. The *lines* are CNLS fits to the data using the circuit model of Fig. 8b. The insets show magnified views of the high frequency spectra on optimized scales

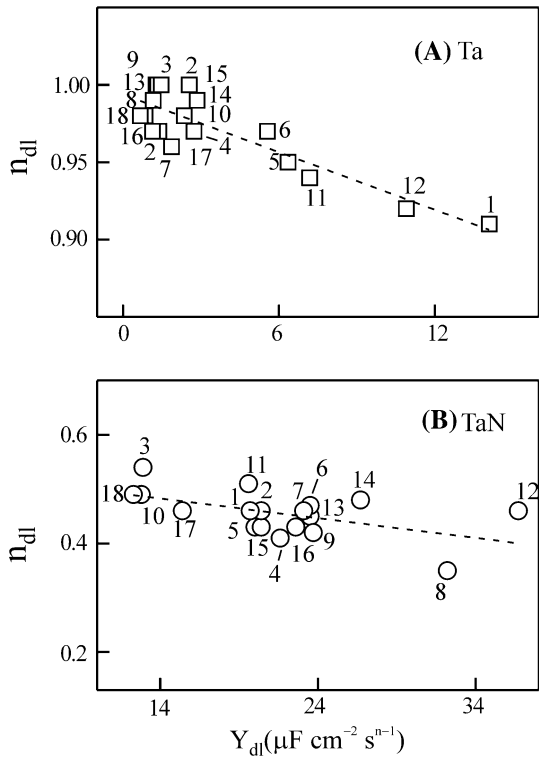

Fig. 10 Interdependent trends of n_{dl} and Y_{dl} for **a** Ta and **b** TaN electrodes in different oxyanion-based solutions. The *squares* in (**a**) and the *circles* in (**b**) represent CPE parameters obtained from CNLS analyses of the experimental EIS data considered in Figs. 7 and 9, respectively. The numbers used to label the *symbols* denote experimental solutions listed in Table 1 using the corresponding numbers. The *dashed lines* are least square fits to the compiled data

the value of n_{dl} also represents increasing inhomogeneity of the surface, and for this reason, the system dependent values of n_{dl} and Y_{dl0} vary in mutually opposing directions. Nevertheless, the comparative roles of the various factors that dictate the values of Y_{dl0} and n_{dl} can be quite different for different systems. These factors, which include two- and three-dimensional in-homogeneities of chemical as well as morphological origins [9, 49], do not seem to play strong overlapping roles here in governing the two double-layer CPE parameters. This is indicated by the fact that the linear fits to the data shown in Fig. 10a and b yield fairly small R^2 values of 0.67 and 0.30, respectively.

According to Fig. 8, anion adsorption on Ta is characterized by a single relaxation time τ_{ad} and by two separate time constants, τ_{ad1} and τ_{ad2}, in the case of TaN. The CNLS-analyzed circuit parameters can be used to calculate these time constants: $\tau_{ad}(\text{Ta}) = (R_{ad}Y_{ad})^{1/n}$ [9, 49], $\tau_{ad1}(\text{TaN}) = R_{ad1}C_{ad1}$, and $\tau_{ad2}(\text{TaN}) = R_{ad2}C_{ad2}$. These results for τ_{ad}(Ta), τ_{ad1}(TaN), and τ_{ad2}(TaN) are presented in Figs. 11, 12a–c, and d–f, respectively. The open bars in Fig. 11 show that in H_2O_2-free solutions, τ_{ad}(Ta) for SO_4^{2-} is the lowest among the systems considered, and remains essentially invariant between pH 3 and 6. This in turn suggests that the adsorption of SO_4^{2-} is more efficient than those of NO_3^- and $H_2PO_4^-$ on Ta, where the surface coverage of SO_4^{2-} probably stays at its saturation value in the entire pH range tested in Fig. 11.

The binding configurations of oxyanions adsorbed on metal oxides exhibit pH (surface charge)-dependent variations [51]. However, due to its tightly packed adsorption geometry, the adsorption configuration of SO_4^{2-} on Ta/Ta_2O_5 established at near-saturation surface coverage should be independent of such effects, especially if the solution pH is varied over a relatively small range. Thus, the open bars for K_2SO_4 remain almost unchanged among Fig. 11a, b, and c. On the other hand, because NO_3^-

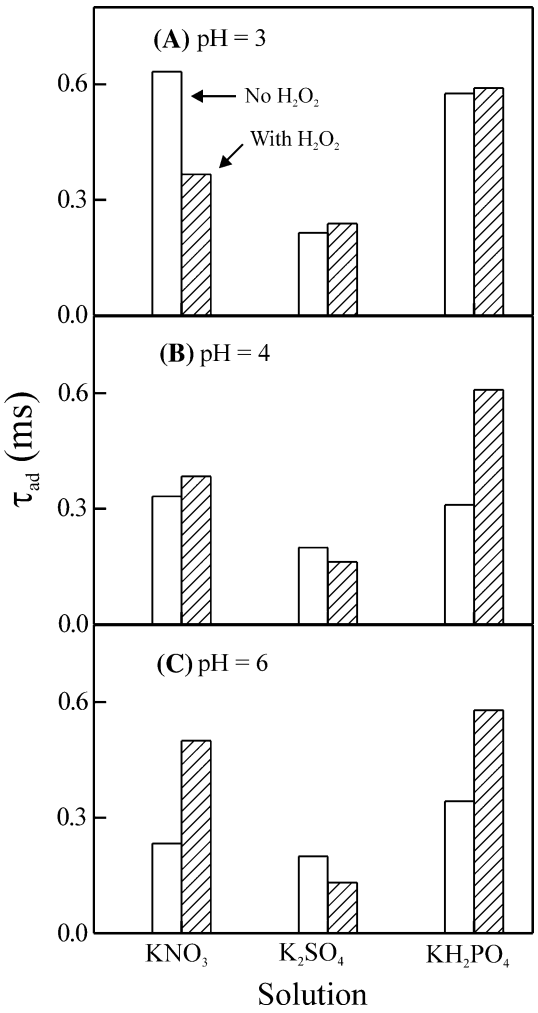

Fig. 11 Solution dependence of the time constant (τ_{ad}) for oxyanion adsorption on Ta obtained from CNLS analyzed values of the C_{ad} and R_{ad} measured at OCPs. The *open* and the *striped bars* represent solutions without and with 5 wt% H_2O_2, respectively

and $H_2PO_4^-$ are likely to exhibit weaker adsorption [52], the surface speciation characteristics of these anions should be relatively more pH dependent. This is manifested in the pH-sensitive behaviors of τ_{ad}(Ta) for KNO_3 and KH_2PO_4 in Fig. 11, where the open bars for both these systems become gradually smaller with increasing pH. The latter effect can be attributed to decreasing amounts of anion-HO_3^+ co-adsorption as the H^+ contents of the solutions drops with increasing pH.

While the open bars in Fig. 11 represent Ta samples only containing native oxides, the corresponding striped bars represent surfaces containing both native and H_2O_2 generated oxides. A comparison of these two sets of data show that, for KH_2PO_4 at pH 3 and for K_2SO_4 at pH 3–6, there are no significant differences between the values of τ_{ad}(Ta) measured with and without H_2O_2 in the solutions. Therefore, for these particular systems, the native oxide layers formed on Ta in the H_2O_2-free solutions are dense enough to efficiently block out any PZC-controlled contributions of the un-oxidized Ta to the net surface charge. The IEP of the surface oxide becomes the main governing factor for the surface charges (and hence the adsorption relaxation times) in these cases. As expected, additional changes to these charges remain minimal as more oxide species of the same chemical makeup (Ta_2O_5) is deposited by reaction (13). In contrast, for KH_2PO_4 at pH 4 and 6, and for KNO_3 at pH 3–6, τ_{ad}(Ta) changes with the addition of H_2O_2. Here, both the PZC of Ta and the IEP of Ta_2O_5 seem to control the net charge of the Ta/Ta_2O_5 surface in the H_2O_2-free solutions, and the IEP becomes more critical in dictating the surface charges of the electrodes in H_2O_2-containing solutions [51].

The relatively small values of τ_{ad}(Ta) observed in Fig. 11 are typical of strong/fast chemisorptions [27, 41]. In comparison with τ_{ad}(Ta), the values of τ_{ad1}(TaN) and τ_{ad2}(TaN) in Fig. 12 are about an order of magnitude larger and lower, respectively. Based on the observations made from Fig. 11, tentatively, the results in Fig. 12a–c and those in Fig. 12d–f can be associated with Ta-deficient and Ta-rich sites of tantalum nitride, respectively. Oxide formation on the Ta-rich sites at E_{oc} is likely to be coupled with anion incorporation, as described, for example, in Eq. 18, and hence the associated values of τ_{ad2}(TaN) are small. According to Eq. 20, the Ta-deficient surface sites of tantalum nitride would mostly be un-oxidized TaN in H_2O_2-free solutions, and TaON in H_2O_2-added solutions. These TaN and TaON may dominate the behavior of τ_{ad1}(TaN) represented by open- and striped bars in Fig. 12, respectively. Owing to the different adsorption chemistries of the TaN/TaON (Fig. 12a–c) and Ta_2N/Ta_2O_5 (Fig. 12d–f), the adsorption times, τ_{ad1}(TaN) and τ_{ad2}(TaN), of the three oxyanions exhibit different individual values in the two cases.

3.9 Utility of oxyanion-induced surface modification in chemically promoted CMP

The foregoing EIS data, in combination with those shown in Figs. 4, 5, 6, demonstrate how oxyanion incorporated surface oxides can be formed on Ta and TaN during CMP in the absence of external anodic activation. This structural weakening of Ta/TaN surface layers occurs through chemical/electrochemical routes but do not rely on uncontrolled material dissolution reactions. In addition, unlike the case of halide ions, oxyanions do not generally cause pitting corrosion on metal/alloy substrates of their adsorption [26]. These are essential criteria for reducing surface defects in CMP, and initial efforts to explore oxyanion chemistries for low-pressure CMP have shown promising results [4, 5]. Some of the main experimental

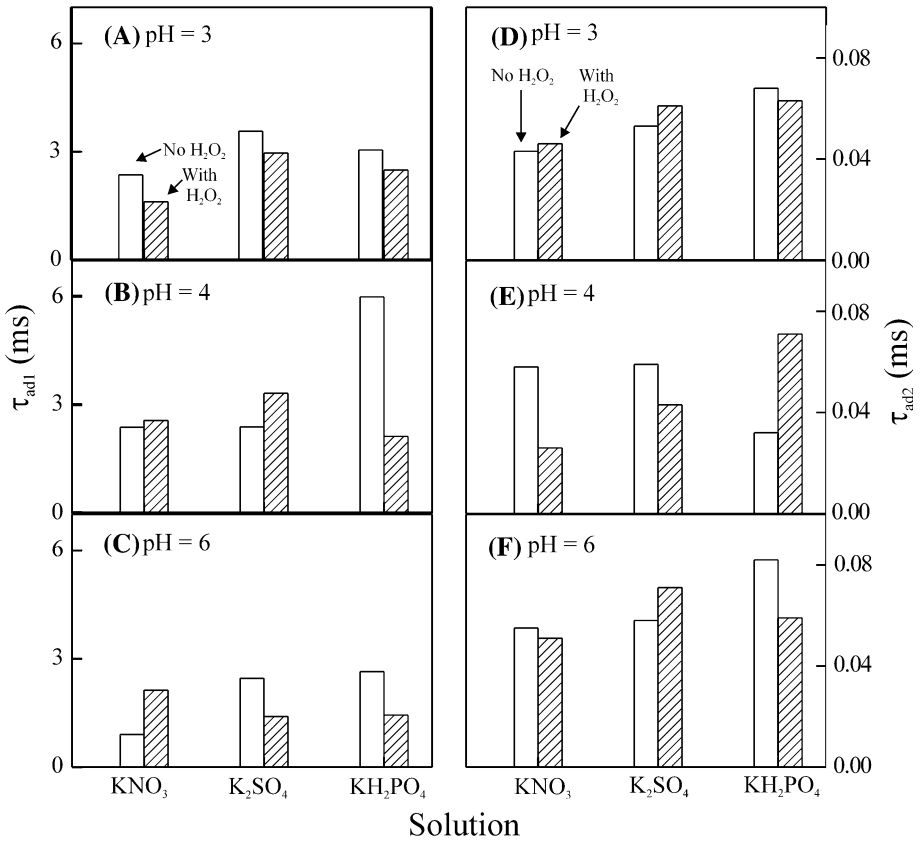

Fig. 12 Solution-dependent characteristic times τ_{ad1} (in **a–c**) and τ_{ad2} (in **d–f**) for oxyanion adsorption on Ta-deficient and Ta-rich sites of tantalum nitride, respectively. In each panel, the *open* and the *striped bars* represent solutions without and with 5 wt% H_2O_2, respectively

considerations for using this specific CMP strategy are briefly noted below in light of the recently reported PR and defectivity data for such systems.

Typical CMP steps used in the processing of Cu damascene structures consist of bulk Cu removal (step-1) followed by selective removal of residual Cu, Ta/TaN barrier layers, and SiO_2-based hard mask, as well as controlled partial deletion of the underlying low-k dielectric (step-2). Oxyanion-based CMP slurries are likely to find their main applications in the area of step-2 CMP. With the reduced diffusion barrier layers thicknesses ($\leq$5 nm) [2] designed for the new technology nodes, Ta/TaN removal rates of 30–50 nm min^{-1} should adequately support this second step of CMP. Because the oxides are continuously formed and removed during CMP, oxyanion incorporation within only a fraction of this polish-depth is sufficient to support low-pressure processing of such systems in a controlled timescale.

Monolayer/sub-monolayer amounts of modified surface oxides necessary to support low pressure CMP in real time can result from moderate potentials (excess surface charge) [17]. For instance, native surface oxides of Ta typically are found as 2.5–3.0 nm thick layers [53], and a surface potential of 0.2 V can establish an electric field of $\sim 10^8$ V m^{-1} across such a layer. Previous experiments [13] using Ta samples under galvanostatic control in H_2SO_4 and H_3PO_4 have shown that surface fields of such magnitude are sufficient to form $\sim$20–70 nm thick anion incorporated Ta-oxide films in a timeframe of 50–150 s, depending on the anion content and concentration of the experimental solution. Up to 70% of the total oxide-layer thickness grown under these conditions has been found to be oxyanion doped [13].

In the aforementioned cases of electrically controlled continuous oxidation, the rate of oxide growth decreases with increasing values of d in the exponential term of Eq. 6. On the other hand, in the actual CMP situation, where the generation of the oxide film is coupled with immediate removal of the latter, the rate of oxide-induced surface modification should be more efficient. Thus, even with relatively low concentrations (0.03–0.07 M) of oxyanions [4], it should be possible, in real time during CMP, to continuously generate a fresh monolayer of anion incorporated oxides at the surface of the polishing pad. This in turn should sustain a satisfactory polish rate of Ta/TaN during the CMP process. The recent results of Ta CMP reported by Surisetty et al. [4, 5] are in full agreement with this view, where 30–50 nm min PRs of Ta blanket wafers have been achieved at 2 psi down pressure, with slurry solutions containing various oxyanions in the concentrations of 0.065–0.130 M, and by employing typical values of the other control variables for step-2 CMP.

Selective removal of Cu under pH control has also been observed in the aforementioned experiments, and optically monitored roughness parameters of the processed Ta and Cu wafers have shown a satisfactory level of defect suppression [5]. Subsequent studies have examined the experimental variables (platen speed, pad conditioning, as well as oxianion and oxidizer concentrations, solution pH, abrasive content, and flow rate of the slurry) necessary to improve selective PRs and defectivity for these CMP systems [4]. It has been found in this context that high concentrations of oxyanions did not necessary increase Ta PRs while using SiO_2 abrasives in weakly acidic slurries. For instance, in a second-step CMP slurry containing K_2SO_4 + 1wt% H_2O_2 + 8 wt% SiO_2 at pH 4, a critical concentration of 0.032 M K_2SO_4 was necessary to polish Ta wafers at 79 nm min^{-1} using 2 psi down pressure. This PR only varied moderately between 70 and 86 min^{-1}, as the sulfate content of the slurry was increased up to 0.25 M, with the maximum PR occurring at $[SO_4^{2-}] = 0.065$ M. With further increments in $[SO_4^{2-}]$, the Ta PRs dropped, possibly because the anions adsorbed on Ta/Ta_2O_5 at higher ion concentrations affected substrate interactions with the SiO_2 (IEP $\approx$ 3.5 [44]) abrasives. Based on these observations, the surface chemistry of the abrasive particles should also be considered along with that of the substrate material while designing oxyanion-based CMP slurries.

Because defectivity and dishing are particularly important issues for CMP of patterned wafers, a model oxyanion system, namely, a sulfate-based slurry composition (0.065 M K_2SO_4 + 1 wt% H_2O_2 + 8 wt% SiO_2 at pH 4), has been studied in detail by Surisetty for step-2 CMP of patterned wafers designed for the 32-nm Cu technology [4]. These CMP experiments were performed using an ex-situ conditioned soft pad at a down pressure of 2.2 psi, and the processed wafers were checked for defects using optical profilometry as well as a defect-review tool incorporating scanning electron microscopy (SEM). The details of these studies have been discussed elsewhere, and the results have been promising [4]. In brief, the sulfate-based test slurry supported selective polishing of the Ta/TaN barrier layer, as well as the hard mask, while supporting a relatively small rate for controlled removal of the low-k. When the sulfate-based slurry was used after bulk Cu removal with a commercial Cu slurry, the post-polish wafers were noticeably defect-free, and a significant degree of dishing correction ($\sim$20–30 nm) was achieved [4].

4 Conclusions

The strategy of using oxyanions as surface-modifying agents for barrier CMP [4] is aligned with the new ITRS recommendations, and has potentials for large-scale incorporation in the processing of low-k-based interconnect structures. This study provides a detailed electrochemical investigation of the mechanism of this CMP method for Ta and TaN. The results demonstrate how the solution-dependent behaviors of the electrochemical parameters of these systems can be linked to corresponding slurry chemistries for CMP. This, in turn, also underscores the utility of electro-analytic techniques for the characterization of novel CMP systems. The electrochemical results discussed here demonstrate that with adequate experimental designs, such chemically/structurally modified oxides can be generated on both Ta and TaN for CMP applications. Structural changes in these oxides occur through anion incorporation, which forms chemically/structurally modified oxide species such as $Ta_2O_{5(1-x)}(NO_3)_{10x}$, $Ta_2O_m(SO_4)_{5x}$, and $Ta_2O_{5(1-x)}(PO_4)10_{x/3}$ in KNO_3, K_2SO_4, and KH_2PO_4 solutions, respectively.

Certain reaction schemes have been proposed here to explain anion-incorporated oxide formation on Ta and TaN. Time-dependent OCP measurements demonstrate how these reactions are sustained during CMP. LPR experiments show that the structural weakening of the surface layers of both Ta and TaN is rooted in their common oxide chemistry. FT-EIS detects detailed differences in the reaction kinetics of these two electrode materials, showing signature effects of both Ta-rich and Ta-deficient sites on TaN, with a single type of adsorption site on Ta. The FT-EIS results also provide supporting evidence for the reaction mechanisms proposed in the context of the D.C. experiments. In addition, the discussions presented here address certain essential aspects of incorporating the strategy of anion-modified oxide formation in the experimental framework of Ta/TaN CMP.

Acknowledgments This study was funded in part by the Semiconductor Research Corporation through IBM and by Clarkson University.

References

1. Krishnan M, Nalaskowski JW, Cook LM (2010) Chem Rev 10:178
2. The International Technology Roadmap for Semiconductors: http://www.itrs.net/Links/2009ITRS/Home2009.htm
3. Chang TC, Mor YS, Liuc PT, Tsabi TM, Chenb CW, Meid YJ, Sze SM (2001) Thin Solid Films 398:523
4. Surisetty CVVS (2010) PhD Thesis, Clarkson University
5. Surisetty CVVS, Peethala BC, Roy D, Babu SV (2010) Electrochem Solid-State Lett 13:H244
6. Stansbury EE, Buchanan RA (2000) Fundamentals of electrochemical corrosion. ASM International, Materials Park
7. Fontana MG (1986) Corrosion engineering. McGraw Hill, New York
8. Sulyma CM, Roy D (2010) Appl Surf Sci 256:2583
9. Barsoukov E, Macdonald JR (2005) Impedance spectroscopy: theory, experiment, and applications. Wiley, New York
10. Zheng JP, Klug BK, Roy D (2008) J Electrochem Soc 155:H341

11. Garland JE, Pettit CM, Roy D (2004) Electrochim Acta 49:2623
12. Sulyma CM (2010) PhD Thesis, Clarkson University
13. Shimizu K, Brown GM, Habazaki H, Kobayashi K, Skeldon P, Thompson GE, Wood GC (1998) Corros Sci 40:963
14. Wood GC, Skeldon P, Thompson GE, Shimizu K (1996) J Electrochem Soc 143:74
15. Lu Q, Skeldon P, Thompson GE, Masheder D, Habazaki H, Shimizu K (2004) Corros Sci 46:2817
16. Kerrec O, Devilliers D, Groult H, Chemla M (1995) Electrochim Acta 40:719
17. Assiongbon KA, Emery SB, Pettit CM, Babu SV, Roy D (2004) Mater Chem Phys 86:347
18. Young L (1961) Anodic oxide films. Academic, New York
19. Bartels C, Schultze JW, Stimming U, Habib MA (1982) Electrochim Acta 27:129
20. Hug SJ (1997) J Colloid Interface Sci 188:415
21. Weber M, Nart FC, de Moraes IR (1996) J Phys Chem 100:19933–19938
22. Goldberg S, Sposito G (1985) Commun Soil Sci Plant Anal 16:801
23. Milazzo G, Caroli S (1978) Tables of standard electrode potentials. Wiley, New York
24. Goonetilleke PC, Roy D (2005) Mater Chem Phys 94:388
25. Pagitsas M, Diamantopoulou A, Sazou D (2001) Electrochem Commun 3:330
26. Sulyma CM, Roy D (2010) Corros Sci 52:3086
27. Pell WG, Zolfaghari A, Conway BE (2002) J Electroanal Chem 532:13
28. Majima M, Awakura Y, Yazaki T, Chikamori Y (1980) Metall Trans B 11:209
29. Martyak NM, Ricou P (2004) Mater Chem Phys 84:87
30. Wang YS, Lee WH, Wang YL, Hung CC, Chang SC (2008) J Phys Chem Solids 69:601
31. Cuong ND, Kim DJ, Kang BD, Kim CS, Yu KM, Yoon SG (2006) J Electrochem Soc 153:G164
32. Min KH, Chun KC, Kim KB (1996) J Vac Sci Tech B 14:3263
33. Ritala M, Kalsi P, Riihelä D, Kukli K, Leskelä M, Jokinen J (1999) Chem Mater 11:1712
34. Wang Z, Yaegashi O, Sakaue H, Takahagi T, Shingubara S (2003) J Appl Phys 94:4697
35. Liao CN, Liou KM (2005) J Vac Sci Tech A23:359
36. Chung HC, Liu CP (2006) Surf Coat Tech 200:3122
37. Kuo YL, Huang JJ, Lin ST, Lee C, Lee WH (2003) Mater Chem Phys 80:690
38. Arranz A, Palacio C (1994) Vacuum 45:1091
39. Ibidunni AO, MaSaitis RL, Opila RL, Davenport AJ, Isaacs HS, Taylor JA (1993) Surf Interface Anal 20:559
40. Janjam SVSB, Peethala BC, Roy D, Babu SV (2010) Electrochem Solid-State Lett 13:H1
41. Walters MJ, Pettit CM, Roy D (2001) Phys Chem Chem Phys 3:570
42. Goonetilleke PC, Roy D (2008) Appl Surf Sci 254:2696
43. McCafferty E, Wightman JP (1977) J Colloid Interface Sci 194:344
44. Kosmulski M (2004) J Colloid Interface Sci 275:214
45. Kosmulski M (1997) Langmuir 13:6315
46. Vermilyea A (1965) J Electrochem Soc 112:1232
47. Mikolajick T, Kühnhold R, Ryssel H (1997) Sens Actuators B 44:262
48. Ammar IA, Ismail IK (1972) Mater Corrs 23:168
49. Orazem ME, Tribollet B (2008) Electrochemical impedance spectroscopy. Wiley, New York
50. Janjam SSB, Peethala BC, Zheng JP, Babu SV, Roy D (2010) Mater Chem Phys 123:521
51. Hiemstra T, Van Riemsdijk WH (1999) J Colloid Interface Sci 210:182
52. Melendres CA, Hahn F, Bowmaker GA (2000) Electrochim Acta 46:9
53. Sung YE, Bard, AJ (1998) J Phys Chem B 102:9806